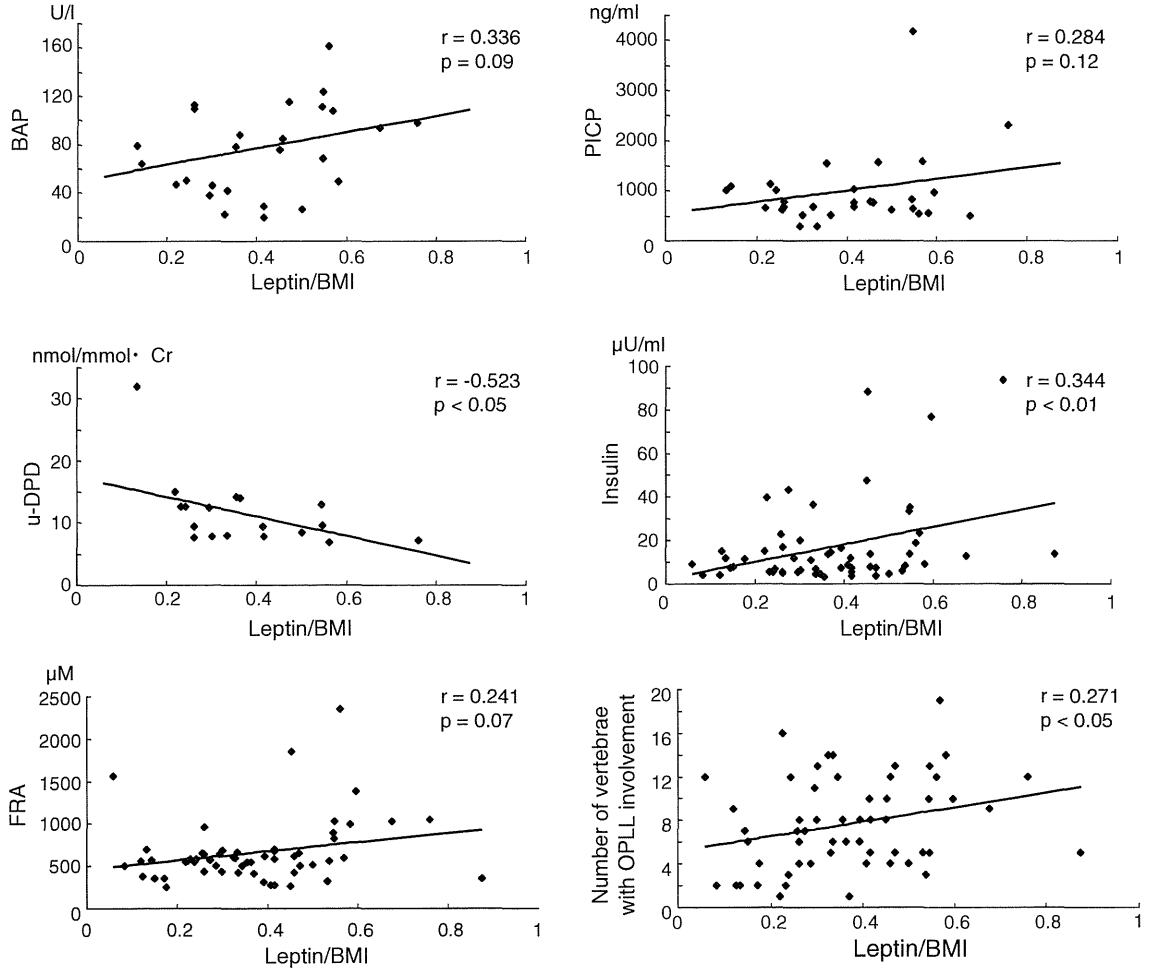

Fig. 2 Relationship between the leptin/BMI (body mass index) ratio and bone metabolic markers including serum bone-specific alkaline phosphatase (BAP), carboxyterminal propeptide of type I procollagen (PICP), and urine deoxypyridinoline (DPD), serum insulin and fructosamine (FRA) concentrations, and the number of vertebrae with OPLL (ossification of the posterior longitudinal ligament) involvement in female OPLL patients. There was a negative, significant correlation between the leptin/BMI ratio and urine DPD levels, while a positive, significant correlation between the leptin/BMI ratio and serum insulin levels, and the number of vertebrae with OPLL involvement

Correlation of leptin/BMI ratios with bone metabolic markers, serum insulin and FRA concentrations, and the number of vertebrae with OPLL involvement in females with type C-OPLL or type TL-OPLL

To investigate the factors associated with the leptin/BMI ratio in female patients with type TL-OPLL, we examined the correlation between leptin/BMI ratios and bone metabolic markers, serum insulin and FRA concentrations, and the number of vertebrae with OPLL involvement (Fig. 3). There was a strong, positive correlation between serum BAP levels and the leptin/BMI ratio ($r = 0.518, p < 0.05$), but no significant difference between PICP levels and the ratio. Urine DPD and serum FRA levels, and the number of vertebrae with OPLL involvement did not show a significant correlation with the leptin/BMI ratio. Interestingly, serum insulin concentrations correlated positively with the leptin/BMI ratio ($r = 0.324, p < 0.05$). We also carried out similar correlation analyses on type C-OPLL females, but found no significant relationship between the variables (data not shown).

Discussion

This study demonstrated that females with OPLL had significantly higher serum leptin levels compared with females without OPLL and that the levels correlated positively with serum insulin levels. These findings are consistent with those of a previous study by Shirakura et al. [24]. In the present study, we carried out further investigations to determine the factors associated with the leptin/BMI ratio in OPLL females and showed that urine DPD concentrations correlated negatively with the ratio. This

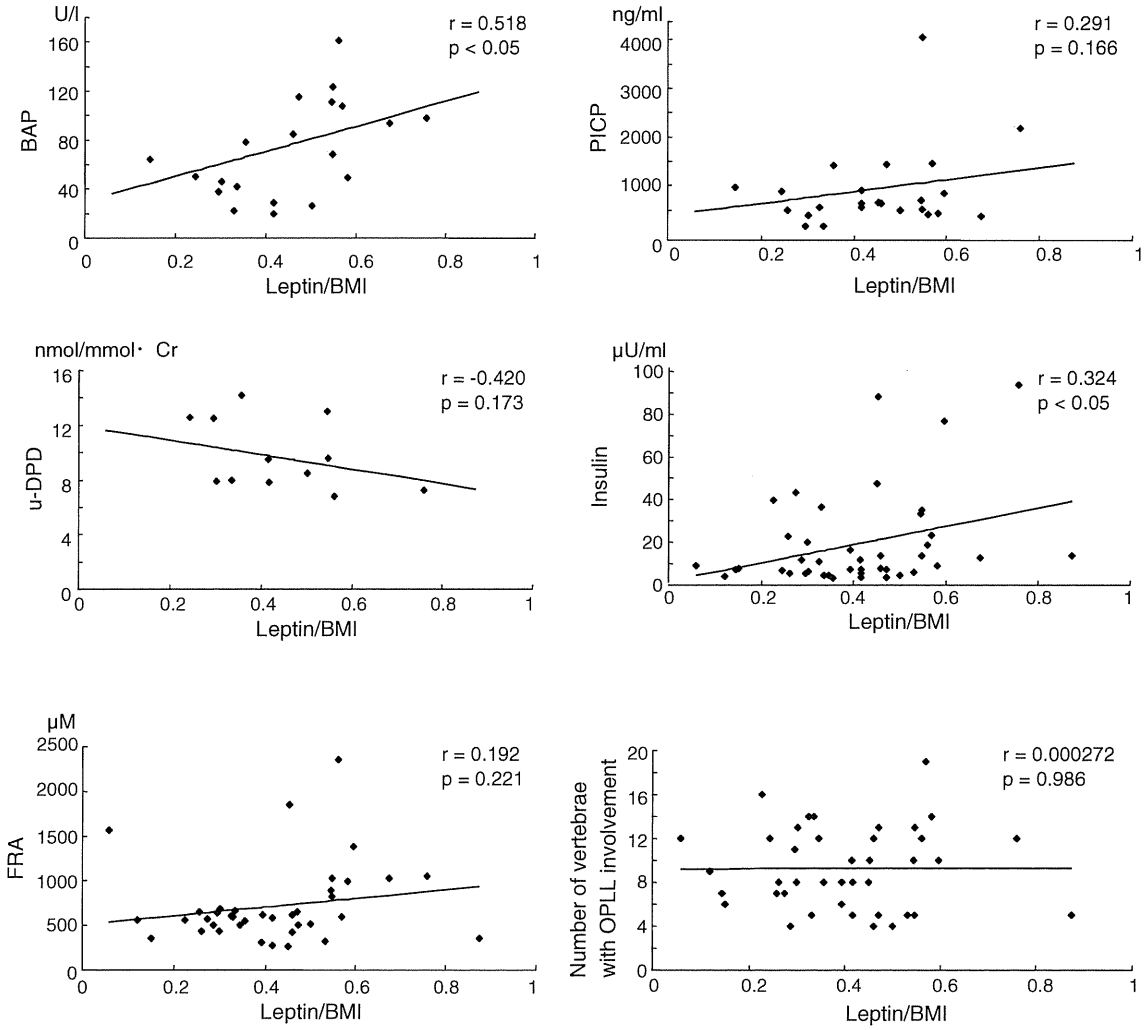

Fig. 3 Relationship between the leptin/BMI (body mass index) ratio and bone metabolic markers including serum bone-specific alkaline phosphatase (BAP), carboxyterminal propeptide of type I procollagen (PICP), and urine deoxypyridinoline (DPD), serum insulin and fructosamine (FRA) concentrations, and the number of vertebrae with OPLL involvement in female type TL-OPLL patients. There was a positive, significant correlation between the leptin/BMI ratio and serum BAP levels, and serum insulin levels

suggests a regulatory effect of leptin on bone resorption, which is in agreement with the report of Burguera et al. [2] who demonstrated in animal experiments that leptin prevented ovariectomy-induced bone loss. Taken together, these results indicate a tendency for a positive correlation between BAP levels and the leptin/BMI ratio in OPLL females and that bone anabolism may be promoted in these patients. However, a significant correlation between urine DPD levels and the leptin/BMI ratio in OPLL females may be influenced by one sample that appears to be an outlier (leptin/BMI = 0.13, u-DPD = 32) as shown in Fig. 2 because this association lost statistical significance when that one sample was excluded ($p = 0.085$, data not shown). Further studies are necessary to establish association between urine DPD levels and the leptin/BMI ratio in OPLL females.

It is interesting that the number of vertebrae with OPLL involvement correlated positively with the leptin/BMI ratio in female patients with OPLL. To the best of our knowledge, there have been no other reports demonstrating an association between serum leptin levels and the extent of OPLL development in humans. We showed previously that the A861G variant in the leptin receptor gene (Ob-R) was associated with more extensive OPLL [29]. Although the effects of the variant in Ob-R on leptin signaling are unknown, this finding suggests that altered leptin signaling in spinal ligament cells may be a factor that regulates the extent of OPLL development.

To date, a few in vitro studies have revealed the mechanisms by which leptin induces osteogenic differentiation in spinal ligament cells [6, 24]. Fan et al. [6] demonstrated that leptin caused significant increases in

mRNA expression of alkaline phosphatase (ALP) and osteocalcin in thoracic ossification of ligament flavum (TOLF) cells, but not in non-TOLF cells, and that the effect was both dose- and time-dependent. These findings suggest that TOLF cells are considerably more sensitive to leptin stimulation and that leptin has the potential to promote osteogenic differentiation in ligament flavum cells. However, this leptin-induced osteogenic differentiation was observed only in response to pharmacological doses, which are not equivalent to physiological concentrations in humans. This implies that ligand stimulation with cytokines, other than leptin, is required to induce osteogenic differentiation in spinal ligament cells.

Insulin has been implicated in the development of heterotopic ossification of spinal ligaments [8, 12, 15]. Spinal ligament cells express insulin receptor substrate (IRS)-1, a common major substrate for both insulin and insulin-like growth factor (IGF)-I receptor tyrosine kinase [12]. We have reported previously that IGF-I stimulates proliferation and collagen type I synthesis in the majority of spinal ligament cells [8]. Li et al. [15] showed that both insulin and IGF-I increased proliferation and ALP activity in human spinal ligament cells. It has been reported that leptin acts through some of the components of the insulin signaling cascade by recruiting several IRSs [1, 7, 9, 19]. This implies that there is cross-talk between leptin signaling and insulin-induced pathways. Our finding that the leptin/BMI ratio correlated positively with serum insulin levels in OPLL females suggests that increased levels of both leptin and insulin may act synergistically to strengthen downstream signaling, thereby contributing to the development of OPLL.

As the number of vertebrae with OPLL involvement correlated positively with serum leptin levels in OPLL females, we hypothesized that female patients with extended OPLL may have higher serum levels of leptin than those with limited OPLL. To verify this hypothesis, we divided the OPLL females into two further subgroups; type C and type TL groups. We then compared BMI, serum leptin levels, leptin/BMI ratios, and serum insulin and FRA concentrations in these two groups. The results showed that relative to type C-OPLL, serum leptin levels and leptin/BMI ratios were increased significantly in type TL-OPLL by 1.6- and 1.9-fold, respectively. Although there were no statistical differences in serum insulin and FRA concentrations between the groups, higher levels of insulin and FRA were detected in type TL-OPLL, which supports the concept that both hyperleptinemia and hyperinsulinemia contribute to extension of heterotopic ossification of the spinal ligament in OPLL females.

It is also of interest that there was a positive, significant correlation between the leptin/BMI ratio and BAP levels in type TL-OPLL females whose serum leptin concentrations were significantly higher than type C-OPLL, whereas no significant correlation was detected in all OPLL females. These results indicate that bone anabolism is elevated substantially in female type TL-OPLL patients compared to female type C-OPLL patients. However, this is inconsistent with a previous report that serum leptin levels are negative regulators of bone mass [5]. We speculate that in OPLL females there may be a decrease in leptin sensitivity in the hypothalamus, which in turn, increases circulating leptin levels, resulting in the development of OPLL through the direct and anabolic effects of leptin on bone and spinal ligament cells.

OPLL occurs frequently at the cervical spine [33]. However, it has not been determined why OPLL is sometimes limited to the cervical spine or alternatively extends to the thoracic and/or lumbar spine. As shown in our study, higher serum leptin levels, detected in female patients with OPLL extending to the thoracic and/or lumbar spine, may be a causative factor determining the extension of OPLL. However, even if serum leptin levels or other systemic factors including serum insulin or FRA levels affect the extension of OPLL, there still remains the question as to why the limited type of OPLL is seen frequently at the cervical spine. We speculate that mechanical stress, which is supposedly a local factor, could be a prime candidate to induce heterotopic ossification in the cervical spine but is unlikely to occur in the thoracic spine. Iwasawa et al. [11] demonstrated that exposure to mechanical stress such as uniaxial stretching upregulated various genes related to bone metabolism including endothelin-1 (ET-1) and prostaglandin I_2 (PGI_2) in OPLL cells. This shows clearly the importance of mechanical stress in heterotopic ossification of the spinal ligament. Several biomechanical studies have revealed that the range of motion (extension and flexion) of the cervical spine is much larger than that of the thoracic spine [18, 27, 35]. Taken together, it is conceivable that moderately elevated levels of leptin, in combination with mechanical stress to the ligament cells, may contribute to the development of cervical OPLL, while highly elevated levels of leptin may have a role in the extension of OPLL to the thoracic and/or lumbar spine.

The important issue that is not clarified by the present study is the significant gender difference between serum leptin levels and the development of OPLL. It is likely that some gender-specific factors such as estrogen may have an important role in the development of OPLL. Recent studies on human periodontal ligament cells have shown that estrogen is capable of inducing osteogenic differentiation in ligament cells [16, 25, 38]. It has also been shown previously in the Japanese population that serum estrogen levels are elevated significantly in OPLL patients, and that the levels are related to the extent of heterotopic ligament ossification [34]. These observations suggest a pivotal role

for estrogen in heterotopic ossification of the spinal ligament. We therefore speculate that serum leptin do not regulate solely the development of OPLL, but may contribute to the development of OPLL in combination with some gender-specific factors such as estrogen.

In summary, we showed that serum leptin concentrations are elevated in females with OPLL and are associated with extension of OPLL, i.e. an increased number of vertebrae with OPLL involvement. In addition, serum leptin levels in patients with extensive OPLL (thoracic and/or lumbar type) were higher than in patients with limited OPLL (cervical type). These observations indicate that hyperleptinemia may contribute to the development of heterotopic ossification of the spinal ligament in females with OPLL. However, it is also clear that this scenario does not completely explain the entire mechanism of spinal ligament ossification in OPLL patients as other complicated pathological factors associated with OPLL such as hyperinsulinemia, hyperlipidemia, and high glucose levels coexist with hyperleptinemia. The present observations are, nevertheless, important for future work and may provide information on the mechanisms underlying the development of OPLL, and ultimately may lead to potential drug therapies for management of this disease.

Acknowledgments This study was supported by a Grant-in-Aid for Scientific Research from the Ministry of Education, Science and Culture of Japan, and by a grant for Intractable Diseases from the Public Health Bureau, the Ministry of Health and Welfare of Japan (Investigation Committee on Ossification of the Spinal Ligaments).

References

1. Benomar Y, Roy AF, Aubourg A, Djiane J, Taouis M (2005) Cross down-regulation of leptin and insulin receptor expression and signaling in a human neuronal cell line. Biochem J 388:929–939
2. Burguera B, Hofbauer LC, Thomas T, Gori F, Evans GL, Khosla S, Riggs BL, Turner RT (2001) Leptin reduces ovariectomy-induced bone loss in rats. Endocrinology 142:3546–3553
3. Cornish J, Callon KE, Bava U, Lin C, Naot D, Hill BL, Grey AB, Broom N, Myers DE, Nicholson GC, Reid IR (2002) Leptin directly regulates bone cell function in vitro and reduces bone fragility in vivo. J Endocrinol 175:405–412
4. Ducy P, Amling M, Takeda S, Priemel M, Schilling AF, Beil FT, Shen J, Vinson C, Rueger JM, Karsenty G (2000) Leptin inhibits bone formation through a hypothalamic relay: a central control of bone mass. Cell 100:197–207
5. Elefteriou F, Takeda S, Ebihara K, Magre J, Patano N, Kim CA, Ogawa Y, Liu X, Ware SM, Craigen WJ, Robert JJ, Vinson C, Nakao K, Capeau J, Karsenty G (2004) Serum leptin level is a regulator of bone mass. Proc Nat Acad Sci 101:3258–3263
6. Fan D, Chen Z, Chen Y, Shang Y (2007) Mechanistic roles of leptin in osteogenic stimulation in thoracic ligament flavum cells. J Biol Chem 282:29958–29966
7. Fruhbeck G, Salvador J (2000) Relation between leptin and the regulation of glucose metabolism. Diabetologia 43:3–12
8. Goto K, Yamazaki M, Tagawa M, Goto S, Kon T, Moriya H, Fujimura S (1998) Involvement of insulin growth factor I in development of ossification of the posterior longitudinal ligament of the spine. Calcif Tissue Int 62:158–165
9. Hegyi K, Fulop K, Kavacs K, Toth S, Falus A (2004) Leptin-induced signal transduction pathways. Cell Biol Int 28:159–169
10. Iida M, Murakami T, Ishida K, Mizuno A, Kuwajima M, Shima K (1996) Substitution at codon 269 (glutamine-proline) of the leptin receptor (OB-R) cDNA is the only mutation found in the Zucker fatty (*fa/fa*) rat. Biochem Biophys Res Commun 224: 597–604
11. Iwasawa T, Iwasaki K, Sawada T, Okada A, Ueyama K, Motomura S, Harata S, Toh S, Furukawa KI (2006) Pathophysiological role of endothelin in ectopic ossification of human spinal ligaments induced by mechanical stress. Calcif Tissue Int 79:422–430
12. Kadowaki T, Tobe K, Honda-Yamamoto R, Tamemoto H, Kaburagi Y, Momomura K, Ueki K, Takahashi Y, Yamauchi T, Akanuma Y, Yazaki Y (1996) Signal transduction mechanism of insulin and insulin-like growth factor-1. Endocr J 43(Suppl): S33–S41
13. Kawai K (1989) Ossification of the insertion of the spinal ligament (Enthesis) in Zucker fatty rats and the effects of ethane-1-hydroxy-1, 1-diphosphonate (EHDP) on its rat. J Tokyo Med Coll 47:558–567 (in Japanese)
14. Kennedy A, Gettys TW, Watson P, Wallace P, Ganaway E, Pan Q, Garvey WT (1997) The metabolic significance of leptin in humans: gender-based differences in relationship to adiposity, insulin sensitivity, and energy expenditure. J Clin Endocrinol Metab 82:1293–1300
15. Li H, Liu D, Zhao CQ, Jiang LS, Dai LY (2008) Insulin potentiates the proliferation and bone morphogenetic protein-2-induced osteogenic differentiation of rat spinal ligament cells via extracellular signal-regulated kinase and phosphatidylinositol 3-kinase. Spine 33:2349–2402
16. Liang L, Yu JF, Wang Y, Wang G, Ding Y (2008) Effect of estrogen beta on the osteoblastic differentiation function of human periodontal ligament cells. Arch Oral Biol 53:553–557
17. Maffei M, Halaas J, Ravussin E, Pratley RE, Lee GH, Zhang Y, Fei H, Kim S, Lallone R, Ranganathan S (1995) Leptin levels in human and rodent: measurement of plasma leptin and *ob* RNA in obese and weight-reduced subjects. Nature Med 1:1155–1161
18. Nakamura H (1994) A radiographic study of the progression of ossification of the cervical posterior longitudinal ligament and that of the anterior longitudinal ligament. Nippon Seikeigeka Gakkai Zasshi 68:725–730 (in Japanese)
19. Niswender KD, Schwartz MW (2003) Insulin and leptin revisited: adiposity signals with overlapping physiological and intracellular signaling capabilities. Front Neuroendocrinol 24:1–10
20. Okano T, Ishidou Y, Kato M, Imamura T, Yonemori K, Origuchi N, Matsunaga S, Yoshida H, ten Dijke P, Sakou T (1997) Orthotopic ossification of the spinal ligaments of Zucker fatty rats: a possible animal model for ossification of the human posterior longitudinal ligament. J Orthop Res 15:820–829
21. Phillips MS, Liu Q, Hammond HA, Dugan V, Hey PJ, Caskey CJ, Hess JF (1996) Leptin receptor missense mutation in the fatty Zucker rat. Nature Genet 13:18–19
22. Reseland J, Gordeladze J (2002) Role of leptin in bone growth: central player or peripheral supporter? FEBS Lett 528:40–42
23. Rosenbaum M, Nicolson M, Hirsch J, Murphy E, Chu F, Leibel RL (1996) Effects of gender, body composition, and menopause on plasma concentrations of leptin. J Clin Endocriol Metab 81:3424–3427
24. Shirakura Y, Sugiyama T, Tanaka H, Taguchi T, Kawai S (2000) Hyperleptinemia in female patients with ossification of spinal ligaments. Biochem Biophys Res Commun 267:752–755

25. Shu L, Guan SM, Fu SM, Guo T, Cao M, Ding Y (2008) Estrogen modulates cytokine expression in human periodontal ligament cells. J Dent Res 87:142–147
26. Steppan CM, Crawford DT, Chidsey Frink KL, Ke H, Swick AG (2000) Leptin is a potent stimulator of bone growth in *ob/ob* mice. Regul Pept 92:73–78
27. Takatsu T, Ishida Y, Suzuki K, Inoue H (1999) Radiological study of cervical ossification of the posterior longitudinal ligament. J Spinal Disord 12:271–273
28. Takaya K, Ogawa Y, Isse N, Okazaki T, Satoh N, Masuzaki H, Mori K, Tamura N, Hosoda K, Nakao K (1996) Molecular cloning of rat leptin receptor isoform complementary DNAs: identification of a missense mutation in Zucker fatty (*fa/fa*) rats. Biochem Biophys Res Commun 225:75–83
29. Tahara M, Aiba A, Yamazaki M, Ikeda Y, Goto S, Moriya H, Okawa A (2005) The extent of ossification of posterior longitudinal ligament of the spine associated with nucleotide pyrophosphate gene and leptin receptor gene polymorphisms. Spine 30:877–880
30. Tanaka S (1994) Ossification of the spinal ligaments in Zucker fatty rat. J Tokyo Med Coll 52:19–32 (in Japanese)
31. Tasaka Y, Yanagisawa Y, Iwamoto Y (1997) Human plasma leptin in obese subjects and diabetics. Endocr J 44:671–676
32. Thomas T, Gori F, Khosla S, Jensen MD, Burguera B, Riggs BL (1999) Leptin acts on human marrow stromal cells to enhance differentiation to osteoblasts and to inhibit differentiation to adipocytes. Endocrinology 140:1630–1638
33. Tsuyama N (1984) Ossification of the posterior longitudinal ligament of the spine. Clin Orthop Relat Res 184:71–84
34. Wada A (1995) Affinity of estrogen binding in the cultured spinal ligament cells: an in vitro study using cells from spinal ligament ossification patients. Nippon Seikeigeka Gakkai Zasshi 69:440–449 (in Japanese)
35. White AA, Panjabi MM (1990) Clinical biomechanics of the spine, 2nd edn. Lippincott-Raven, Philladelphia
36. Yamashita T, Murakami T, Iida M, Kuwajima M, Shima K (1997) Leptin receptor of Zucker fatty rat performs reduced signal transduction. Diabetes 46:1077–1080
37. Zhang Y, Proenca R, Maffei M, Barone M, Leopold L, Friedman JM (1994) Positional cloning of the mouse obese gene and its human homologue. Nature 372:425–432
38. Zhou Y, Fu Y, Li JP, Qi LY (2009) The role of estrogen in osteogenic cytokine expression in human periodontal ligament cells. Int J Periodontics Restorative Dent 29:507–513
39. Zucker LM, Antoniades HN (1972) Insulin and obesity in the Zucker genetically obese rat "fatty". Endocrinology 90:1320–1330

ELSEVIER

The Spine Journal 11 (2011) 927–932

THE SPINE JOURNAL

Clinical Study

Evaluation of ossification of the posterior longitudinal ligament by three-dimensional computed tomography and magnetic resonance imaging

Yoshiharu Kawaguchi, MD, PhD*, Aya Urushisaki, MD, Shoji Seki, MD, PhD, Takeshi Hori, MD, Yumiko Asanuma, MD, PhD, Tomoatsu Kimura, MD, PhD

Department of Orthopaedic Surgery, Faculty of Medicine, University of Toyama, 2630 Sugitani, Toyama 930-0194, Japan

Received 31 March 2010; revised 13 December 2010; accepted 12 August 2011

Abstract

BACKGROUND CONTEXT: Detection of ossification of the posterior longitudinal ligament (OPLL) of lesions by lateral radiography is sometimes difficult because the lesions are small. Three-dimensional computed tomography (3D CT) imaging has made it possible to detect lesions not been seen by lateral radiography.

PURPOSE: To evaluate the use of 3D CT in visualizing and classifying OPLL, and the added value of magnetic resonance imaging (MRI) in determining spinal cord compression.

STUDY DESIGN: Prospective case study in an academic department of orthopedic surgery.

PATIENT SAMPLE: Patients with OPLL diagnosed by lateral radiography of the cervical spine from April 2006 to March 2007 were identified.

METHODS: Ossification of the posterior longitudinal ligament visualized lateral radiography was classified according to the existing scheme as continuous, segmental, mixed, or other type. Ossification of the posterior longitudinal ligament visualized by 3D CT was organized into a classification system comprising flat, irregular, or localized types and were compared with the lateral radiographic images. Magnetic resonance imaging was done to determine the extent of spinal cord compression.

RESULTS: All 55 patients (35 men and 20 women; median age, 66 years) with OPLL were enrolled. Of these, 41 (75%) had a type of OPLL as visualized by 3D CT that corresponded with only one type of OPLL as visualized by lateral radiography. In 39 (71%) of 55, the areas of the ossified lesions visualized by 3D CT were the same as those visualized by lateral radiography. In the other 16, the lesions were either too small or too unclear to be visualized by lateral radiography. In all cases, 3D CT imaging showed that the transverse width of OPLL was within the bilateral Luschka joints, which was not noted by lateral radiography. In 13 of the 14 subjects who underwent MRI, spinal cord compression was noted at the superior or inferior edges of the ossified lesions that had been seen by 3D CT.

CONCLUSIONS: Three-dimensional computed tomography visualization of OPLL provided the basis of a classification system, superior to lateral radiography, and provided new information about OPLL. Combining 3D CT with MRI might be useful to provide details about spinal cord compression in OPLL.

Keywords: 3D CT; Cervical spine; OPLL; Spinal cord compression; MRI

Introduction

Ossification of the posterior longitudinal ligament (OPLL) is characterized by replacement of the ligamentous tissue by ectopic new bone formation [1]. Ossification of the posterior longitudinal ligament often causes narrowing of the spinal canal, and it has been recognized as one of the sources of myelopathy, radiculopathy, or both [2].

FDA device/drug status: Not applicable.

Author disclosures: ***YK:*** Nothing to disclose. ***AU:*** Nothing to disclose. ***SS:*** Nothing to disclose. ***TH:*** Nothing to disclose. ***YA:*** Nothing to disclose. ***TK:*** Nothing to disclose.

* Corresponding author. Department of Orthopaedic Surgery, Faculty of Medicine, University of Toyama, 2630 Sugitani, Toyama 930-0194, Japan. Tel.: (81) 76-434-7353; fax: (81) 76-434-5035.

E-mail address: zenji@med.u-toyama.ac.jp (Y. Kawaguchi)

1529-9430/$ - see front matter © 2011 Elsevier Inc. All rights reserved.
doi:10.1016/j.spinee.2011.08.013

EVIDENCE & METHODS

Context
Despite advances in radiographic techniques, simple lateral radiographs are often used to characterize ossification of the posterior longitudinal ligament (OPLL). This article presents a new classification system using three-dimensional computer tomography (3D CT).

Contribution
The authors found that using 3D CT detected approximately 30% more OPLL lesions, which had been missed using simple lateral radiographs.

Implication
The findings suggest 3D CT might provide additional information that is helpful in surgical planning. The utility and prognostic value of the authors' classification system is unknown.

—The Editors

A radiologic study revealed that OPLL is frequently observed in the cervical spine [3]. Based on lateral radiography of the cervical spine, in 1981, the Investigation Committee on the Ossification of Spinal Ligaments of the Japanese Ministry of Public Health and Welfare published criteria to classify ossification into the following types: continuous, segmental, mixed, and other [4] (Fig. 1). This classification facilitates evaluation of the shape of the ossified lesions. However, detecting ossified lesions by lateral radiography is sometimes difficult because these lesions are small.

Imaging technology of the spine has been advanced during the recent decades, allowing the shape of ossified lesions to be more precisely identified. For example, multidetector computed tomography (CT) with 0.75-mm thick slices can precisely detect lesions, and it provides three-dimensional (3D) images. Three-dimensional CT imaging has been reported to be a valuable tool for the diagnostic and therapeutic display of OPLL for surgical intervention [5].

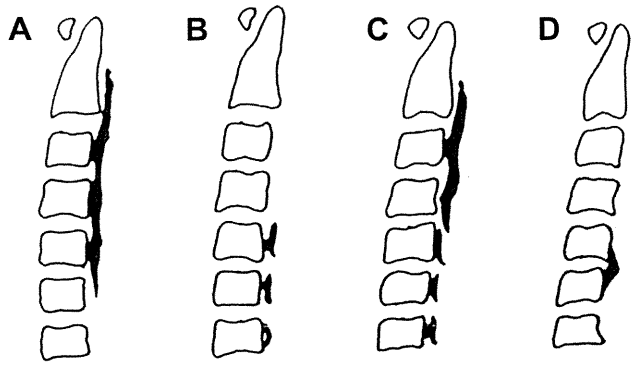

Fig. 1. Proposed classification of ossification of the posterior longitudinal ligament into (A) continuous, (B) segmental, (C) mixed, and (D) other types based on lateral radiographs of the cervical spine [4].

Therefore, we considered the possibility that a new classification of the type of OPLL based on 3D CT may be useful. To evaluate the usefulness of 3D images of OPLL using multidetector CT, images taken by this method were compared with those taken by conventional lateral radiography. In doing so, we sought to determine whether 3D CT could reveal new information about ossified lesions in OPLL. Furthermore, we considered that adding magnetic resonance imaging (MRI) could provide useful information about the extent of spinal cord compression in OPLL.

Materials and methods

From April 2006 to March 2007, 55 consecutive patients with OPLL as diagnosed by lateral radiography of the cervical spine at the University of Toyama Hospital were identified for possible enrollment. This study was approved by the institutional review board of the Faculty of Medicine, University of Toyama, and informed consent was obtained from each patient before enrollment.

Lateral radiographs of the cervical spine were taken in all patients. The presence of OPLL, OPLL type in each vertebra, and intervertebral level from C2 to C6 were determined. Ossification types determined by lateral radiography were classified as continuous, segmental, mixed, and other according to the criteria proposed by the Investigation Committee on the Ossification of Spinal Ligaments of the Japanese Ministry of Public Health and Welfare [4].

Computed tomography images of the cervical spine using a multidetector CT (SOMATOM Sensation 64 Cardiac; Siemens AG, Erlangen, Germany) were also taken for all patients on the same day when lateral radiographs were taken. Specific settings for CT imaging, which were selected to optimize evaluating bony lesions and bone density, were 1 tube rotation/sec; 17.28 mm/sec table feed speed; and 160 milliamperes and 120 kilovolts.

Three-dimensional and multiplanar reconstructions were obtained by use of the CT console (Wizard; Siemens) at 0.5-mm intervals from the 0.75-mm scan slice data. Bone window CT images were used to construct 3D CT images. Laminae of the cervical spine were removed from the computer images, and OPLL was visualized from the posteroanterior view (Fig. 2). The presence of OPLL and its type in each vertebra as well as intervertebral level from C2 to C6 were determined.

Ossification types as determined by 3D CT imaging were classified into three types: flat, irregular, or localized (Fig. 3). In the flat type, flat longitudinally extended ossifications were observed along the posterior margin of both the vertebral body levels and the intervertebral disc levels. The width of the ossification was more than 50% of the spinal canal, and the length was more than three continuous

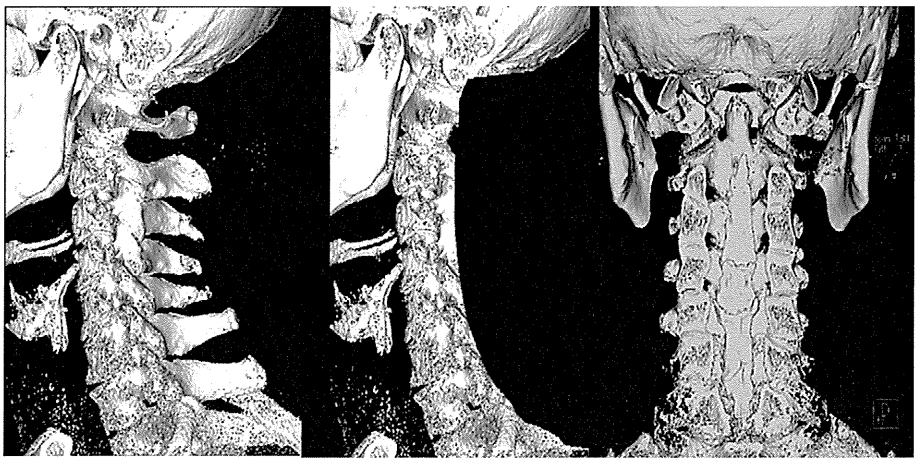

Fig. 2. Use of bone window computed tomography images to construct the three-dimensional image of OPLL in a 66-year-old woman. (Left) posteroanterior view of the cervical spine, (Middle) removal of laminae from computer images, and (Right) visualization of ossification of the posterior longitudinal ligament from the back.

vertebral levels. In the irregular type, irregularly shaped ossifications were observed, such as ossifications only at the bilateral edge of the spinal canal and not in the middle, or ossifications with a double-edged shape. The width of the ossification was less than 50% of that of the spinal canal, and the length was more than three continuous vertebral levels. In the localized type, ossifications were observed only behind the vertebral body or they were not extended more than three continuous vertebral levels.

Preoperative MRI was done in some patients without a history of cervical spine surgery to determine the extent of spinal cord compression. Spinal cord compression was measured by T2-weighted MRI to determine the extent of disappearance of the reserve space in the spinal canal and the deformity of the spinal cord.

Three of the authors (YK, SS, and TH), all spine surgeons, independently evaluated the 3D CT images for OPLL type on two separate occasions. The extent of intrarater agreement was measured by calculation of the kappa statistic (JMP 8; SAS Institute, Cary, NC, USA). The analysts then compared their 3D CT findings, and when they disagreed, they reevaluated the 3D CT images to arrive at a consensus about OPLL type. The extent of interrater agreement was also evaluated by calculation of the kappa statistic.

Then, OPLL type and the longitudinal area of ossified lesions determined by 3D CT imaging were compared with the corresponding findings obtained by lateral radiography. A test to determine the discrepancy in the type of ossification between lateral radiography and 3D CT finding was carried out by Fisher exact test. The one-sample chi-square test was performed to test for the discrepancy between lateral radiography and 3D CT findings in detecting the ossification area of OPLL. These

Fig. 3. Schematic of the various types of ossification of the posterior longitudinal ligament using three-dimensional computed tomography. (Left) Flat, (Middle) irregular, and (Right) localized.

statistical analyses were done with the use of SAS software, Version 9.1. A p value of less than .05 was considered statistically significant.

Results

All 55 patients with OPLL as diagnosed by lateral radiography from April 2006 to March 2007 were enrolled in the study. The enrollees included 35 men and 20 women with a median age of 66 years (range, 48–81 years). Of these enrollees, thirty-five had previously undergone cervical spine surgery by the posterior approach. However, the previous surgery did not reach the OPLL and therefore did not affect the evaluations in this study.

Each of the analysts independently evaluated the 55 3D CT images to determine OPLL type on two separate occasions. For analyst YK, the analyses disagreed one time in the 55 cases, and for analyst SS and TH, the analyses disagreed five times and seven times, respectively. The extent of intrarater agreement between the two separate determinations of OPLL type by 3D CT by an analyst was substantial (kappa statistic value, 0.86 [95% CI=0.78–0.97]).

When the analysts compared their 3D CT determinations to arrive at a consensus of the type of OPLL, they initially disagreed about three cases. In one case, two analysts agreed that OPLL was of the flat type, but the other concluded that the OPLL was of the irregular type. They arrived at a consensus of the flat type. In another case, two analysts agreed that OPLL was of the flat type, but the other concluded that the OPLL was of the localized type. They arrived at a consensus of the flat type. In the third case, two analysts agreed that OPLL was of the irregular type, but the other concluded that the OPLL was of the localized type. They arrived at a consensus of the irregular type. The extent of interrater agreement among the three analysts of OPLL type by 3D CT was substantial (kappa statistic value, 0.78 [95% CI=0.69–0.86]).

The correspondence of the findings regarding the type of OPLL from 3D CT imaging with findings obtained by lateral radiography is shown in Table. Of the 55 patients, 41 (75%) had a type of OPLL as visualized by lateral radiography that corresponded with only one type of OPLL as visualized by 3D CT. That is, for example, all 16 findings of the segmental type and 13 of the mixed-type OPLL as visualized by lateral radiography corresponded only with findings of the localized-type OPLL and irregular-type OPLL, respectively, as visualized by 3D CT images. However, the continuous-type OPLL by lateral radiography corresponded to the flat or the irregular-type OPLL by 3D CT. Statistical analysis showed that this was a significant difference in the type of OPLL as visualized by lateral radiography ($p<.001$).

In 39 (71%) of the 55 cases, areas of the ossified lesions in each vertebra and intervertebral level from C2 to C6 using 3D CT were the same as those using lateral radiography. These 39 cases comprised 12 patients with the flat type, 13 with the irregular type, and 14 with the localized type of OPLL by the evaluation of 3D CT images.

In contrast, in the other 16 (29%) cases, the results between 3D CT and lateral radiography differed. In 9 of these 16, the ossified lesions were too small to be confirmed by radiography but could be observed by 3D CT, which revealed irregular-type OPLL in 5 and localized-type OPLL in 4. In the remaining 7 cases, the discontinuity of the ossified lesions was unclear on radiographic imaging but it could be clearly observed on 3D CT images. Of these seven cases, six had the irregular-type OPLL and one had flat-type OPLL as visualized by 3D CT. The discrepancy between lateral radiography and 3D CT findings in the detection of the ossification area of OPLL was statistically significant ($p<.001$).

In all 55 cases, 3D CT imaging showed that the transverse width of OPLL was within the bilateral Luschka joints and that OPLL never extended above the axial level of the superior tip of the odontoid process. These characteristics were not identified by lateral radiography.

Fig. 4 shows an example of superior visualization of OPLL afforded by 3D CT compared with lateral radiography. It was difficult to visualize ossification of C6 by lateral radiography (Fig. 4, Left). However, the 3D CT imaging showed small ossified lesions at C5 and C6.

Table
The combined analysis of OPLL types using 3D CT images and lateral radiographic images

X-ray 3D CT	Continuous type	Segmental type	Mixed type	Other type
Flat type	12	0	0	0
Irregular type	12	0	13	0
Localized type	0	16	0	2

OPLL, ossification of the posterior longitudinal ligament; 3D CT, Three-dimensional computed tomography.

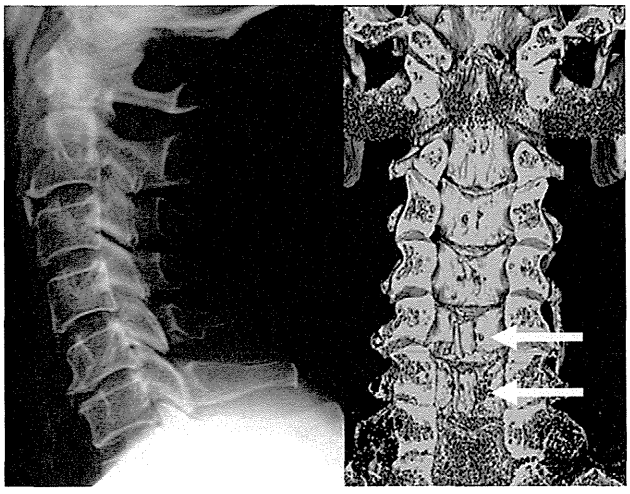

Fig. 4. Images of the cervical spine of a 72-year-old male patient. (Left) Lateral radiograph. (Right) Three-dimensional computed tomography image. The arrows show small ossified lesions at C5 and C6.

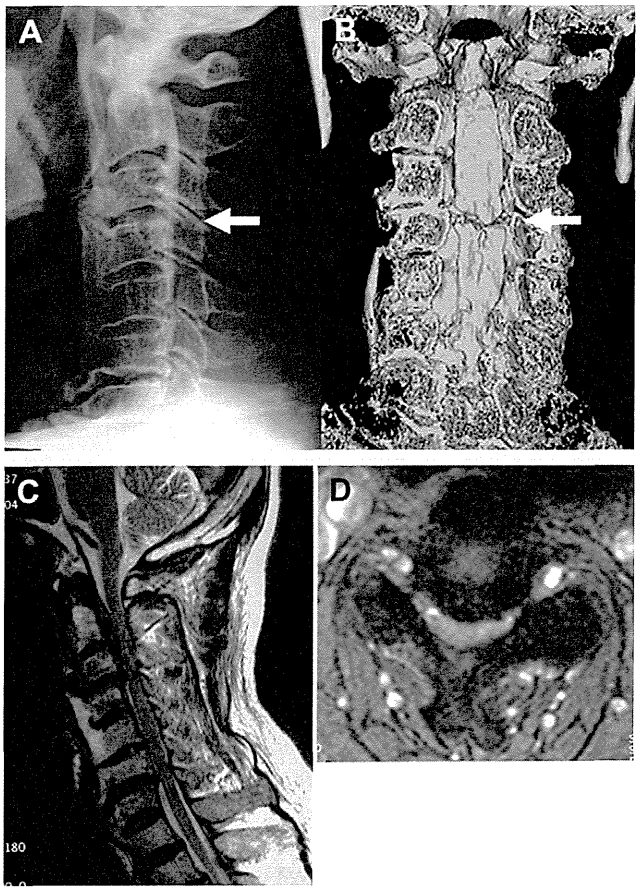

Fig. 5. Images of the cervical spine of a 67-year-old male patient. (A) Lateral radiograph of the cervical spine. (B) Three-dimensional computed tomography prepared from the posterior view of the ossified lesions. (C) Sagittal view of T2-weighted magnetic resonance imaging (MRI). (D) Axial view of T2-weighted MRI at C3–C4. In (C) and (D), the arrows show ossification of the posterior longitudinal ligament at C3–C4.

Of the 14 patients who underwent MRI, 3D CT revealed 7 who had OPLL of the irregular type and 6 who had OPLL of the localized type. In these 13 patients, MRI showed that spinal cord compression was at the superior or inferior edges of the ossified lesions that had been shown by 3D CT. In the other subject, 3D CT revealed the flat type of OPLL, which was thickest at C4 and C5, and MRI revealed that the spinal cord compression was in the middle of the ossified lesion.

Fig. 5 shows an example in which MRI revealed spinal cord compression in a case of OPLL. Based on lateral radiography, continuous OPLL was diagnosed from C2 to C6 (Fig. 5A). However, 3D CT clearly revealed discontinuity of the ossified lesion at C3–C4 (Fig. 5B), and OPLL of the irregular type was diagnosed. A sagittal view of T2-weighted MRI revealed spinal cord compression at C3–C4 (Fig. 5C). Spinal cord compression was marked at C3–C4, where the edge of the ossified lesions was detected on the 3D CT images. An axial view of T2-weighted MRI at C3–C4 showed severe spinal cord compression (Fig. 5D).

Discussion

The advancement of imaging technology and equipment, such as 3D CT, made it possible to detect lesions that had not been previously seen by conventional radiography. Using 3D CT, we presented a new classification scheme for OPLL, and in comparing the findings of 3D CT with those of conventional lateral radiography, we found an interesting difference between these two methods. Analyses of the 3D CT images by three different spine surgeons to determine the type of OPLL substantially agreed, suggesting that our results will be useful for other surgeons.

This study demonstrated the superiority of 3D CT imaging to lateral radiography and revealed new information about the disorder. Findings from MRI complemented the 3D CT findings by revealing the extent of spinal cord compression in OPLL. Three-dimensional computed tomography imaging showed ossified lesions too small to be visualized by lateral radiography, and 3D CT imaging clearly visualized discontinuities that were unclear on lateral radiography. Furthermore, 3D CT revealed new information about OPLL in that 3D CT, and not lateral radiography, showed that the transverse width of OPLL was within the bilateral Luschka joints and that OPLL never extended above the axial level of the superior tip of the odontoid process.

The fact that the transverse width of OPLL was within bilateral Luschka joints that can be attributed to the anatomic features of the posterior longitudinal ligament (PLL). The PLL is attached to the vertebral body and intervertebral disc, and it never extends to the bilateral Luschka joints [6,7]. However, the reason as to why OPLL never extends above the odontoid process remains obscure. The PLL shifts toward the tectorial membrane above the odontoid process [6,7]. The border between the PLL and the tectorial membrane is unclear. A deep layer and thin layer have been identified in the anatomical structure of PLL [6,7]. In contrast, these layers are not found in the tectorial membrane. Thus, the difference between the anatomical features of the PLL and the tectorial membrane might contribute to the cause of OPLL. We are currently examining the detailed structural differences between the PLL and the tectorial membrane.

Ossification of the posterior longitudinal ligament progression has been observed in studies using lateral radiography [8,9]. Although we could observe the precise shape of the ossified lesions using 3D CT, it is unknown how the 3D images of ossified lesions change during long-term progression. The irregular shape of the ossification or the lack of OPLL in the central part in the sagittal plane might indicate OPLL progression. A long-term follow-up study should be carried out to attempt to visualize OPLL progression as visualized by 3D CT imaging.

Three-dimensional computed tomography imaging would also be valuable for surgical simulation of OPLL by increasing the accuracy of surgical procedures.

Hasegawa and Homma [5] described the usefulness of 3D images obtained from helical CT for preoperative simulation in seven patients with OPLL. However, the quality of the images in that report was relatively poor compared with the image quality presently obtainable because of the improvements in imaging technology during recent years. The slice interval in their report [5] was 5 mm, and they did not classify ossified lesions. In contrast, the slice interval in the present report was 2 mm, and the ossified lesions were classified into three types: flat, irregular, and localized.

In conclusion, 3D CT can be the basis for a new classification of OPLL, as it provides new information about the ossified lesions in OPLL. Combining 3D CT with MRI might be useful to detect the patterns, distribution, extent, and cord compression in OPLL. Three-dimensional computed tomography visualization of OPLL was superior to that of lateral radiography, it provided new OPLL information and can be the basis for classification. Combining 3D CT with MRI might be useful to detect the patterns, distribution, extent, and spinal cord compression in OPLL.

Acknowledgments

The authors contracted with Michael S. Altus, PhD, ELS, of Intensive Care Communications, Inc., Baltimore, MD, USA, to edit our initial manuscript. The authors also contacted Drs Hideki Origasa and Shigeki Sumi for the statistical analysis. We thank Drs Altus, Origasa, and Sumi for their excellent services. We maintained complete control over the direction and content of the manuscript.

References

[1] Tsukimoto H. [On an autopsied case of compression myelopathy with a callus formation in the cervical spinal canal]. [in Japanese]. Nihon Geka Hokan 1960;29:1003–7.

[2] Onji Y, Akiyama H, Shimomura Y, et al. Posterior paravertebral ossification causing cervical myelopathy. A report of eighteen cases. J Bone Joint Surg Am 1967;49:1314–28.

[3] Matsunaga S, Sakou T. Ossification of the posterior longitudinal ligament. In: Clark CR, ed. The cervical spine. 4th ed. Philadelphia, PA: Lippincott Williams & Wilkins; 2005:1091–8.

[4] The Investigation Committee on OPLL of the Japanese Ministry of Public Health and Welfare (Tsuyama N). . [The ossification of the posterior longitudinal ligament of the spine (OPLL)]. [in Japanese]. J Jpn Orthop Assoc 1981;55:425–40.

[5] Hasegawa K, Homma T. Morphologic evaluation and surgical simulation of ossification of the posterior longitudinal ligament using helical computed tomography with three-dimensional and multiplanar reconstruction. Spine 1997;22:537–43.

[6] Saifuddin A, Green R, White J. Magnetic resonance imaging of the cervical ligaments in the absence of trauma. Spine 2003;28: 1686–92.

[7] Suzuki Y. [An anatomical study on the anterior and posterior longitudinal ligament of the spinal column. Especially on its fine structure and ossifying disease process]. [in Japanese]. J Jpn Orthop Assoc 1972;46: 179–95.

[8] Kawaguchi Y, Kanamori M, Ishihara H, et al. Progression of ossification of the posterior longitudinal ligament following en bloc cervical laminoplasty. J Bone Joint Surg Am 2001;83:1798–802.

[9] Hori T, Kawaguchi Y, Kimura T. How does the ossification area of the posterior longitudinal ligament progress after cervical laminoplasty? Spine 2006;31:2807–12.

Eur Spine J
DOI 10.1007/s00586-011-2025-x

ORIGINAL ARTICLE

Apoptosis of neurons and oligodendrocytes in the spinal cord of spinal hyperostotic mouse (*twy/twy*): possible pathomechanism of human cervical compressive myelopathy

Kenzo Uchida · Hideaki Nakajima · Shuji Watanabe · Takafumi Yayama · Alexander Rodriguez Guerrero · Tomoo Inukai · Takayuki Hirai · Daisuke Sugita · William E. Johnson · Hisatoshi Baba

Received: 5 January 2011 / Revised: 14 August 2011 / Accepted: 8 September 2011

Abstract
Introduction Cervical compressive myelopathy is the most serious complication of cervical spondylosis or ossification of the posterior longitudinal ligament (OPLL) and the most frequent cause of spinal cord dysfunction. There is little information on the exact pathophysiological mechanism responsible for the progressive loss of neural tissue in the spinal cord of such patients. In this study, we used the spinal hyperostotic mouse (*twy/twy*) as a suitable model of human spondylosis, and OPLL to investigate the cellular and molecular changes in the spinal cord. Mutant *twy/twy* mouse developed ossification of the ligamentum flavum at C2–C3 and exhibited progressive paralysis.
Materials and methods The mutant *twy/twy* mice, aged 16 and 24 weeks, were used in the present study. The cervical spinal cord was analyzed histologically and immunohistochemically.
Results We observed that a significant correlation between the proportion of apoptotic oligodendrocytes in the compressed area of the spinal cord and the magnitude of cord compression. Immunohistochemical analysis indicated overexpression of TNFR1, CD95, and $p75^{NTR}$ in the *twy/twy* mice, which was localized by the immunofluorescence in the neurons and oligodendrocytes.
Conclusion The expression of such factors seems to play at least some role in the apoptotic process, which probably contributes to axonal degeneration and demyelination in the *twy/twy* mice spinal cords with severe compression.

Keywords Apoptosis · Neurons · Spinal cord · Spinal hyperostotic mouse (*twy/twy*) · Chronic compression

Introduction

Compression of the spinal cord may compromise its function and ultimately lead to the appearance of neurological dysfunction and the development of myelopathy, which is also closely correlated with presence of dynamic factors including segmental instability during the spine movement. Cervical compressive myelopathy is the most serious complication of cervical spondylosis and ossification of the posterior longitudinal ligament (OPLL). Mechanical compression and restriction of the cervical spinal cord during the spine movement may result in gait clumsiness, paraesthesia in the hands, gait disturbance as well as signs of posterior and pyramidal column dysfunction; leading eventually to tetraplegia or tetraparesis. Cadaver studies reported that the initial insult could be infarction of the gray matter due to compromise of the spinal cord microvasculature originating at the compression site itself; followed by flattening of the anterior horns, cavity formation, ascending demyelination in the posterior columns, descending demyelination in the lateral columns and proliferation of hyalinized small blood vessels [9, 16, 30]. Since it is difficult to properly estimate and follow the progression of these changes in humans and animal

Electronic supplementary material The online version of this article (doi:10.1007/s00586-011-2025-x) contains supplementary material, which is available to authorized users.

K. Uchida (✉) · H. Nakajima · S. Watanabe · T. Yayama · A. R. Guerrero · T. Inukai · T. Hirai · D. Sugita · H. Baba
Department of Orthopaedics and Rehabilitation Medicine, Faculty of Medical Sciences, University of Fukui, Matsuoka Shimoaizuki 23-3, Eiheiji, Fukui 910-1193, Japan
e-mail: kuchida@u-fukui.ac.jp

W. E. Johnson
Life and Health Sciences, Aston University, Aston Triangle, Birmingham B4 7ET, UK

Published online: 21 September 2011

experimental settings, considerable uncertainty exists regarding the molecular mechanisms responsible for the demyelination that takes place in these disorders, and for the progressive loss of oligodendrocytes and neurons. Such problem is partly related to the lack of an appropriate animal model for investigating the effects of long-term mechanical compression and restriction of the spinal cord.

In a series of studies [3, 4, 23–27], we examined this issue experimentally using the tiptoe-walking Yoshimura (*twy/twy*) mouse, a unique animal that develops spontaneous spinal cord compression without any other reported genetic difference in the anatomy or physiology of the spinal cord that may contribute to the resulting myelopathic syndrome; therefore, directly correlating the clinical behavior to the compression alone, eliminating the multiple factors already mentioned, that may alter the results of our observation. The *twy/twy* mouse is thus suitable for investigating the effects of chronic mechanical compression of the spinal cord, produced without any artificial manipulation of the cord [3, 18]. Using these mice, we reported previously a progressive reduction in the number of anterior horn cells when the transverse remnant area of the spinal cord decreased to ≤70% of the control [3, 4], decreased usage of neurotrophins in autocrine and paracrine interactions [23, 24], and presence of accidental and apoptotic dying spinal cord cells [28, 29]. However, the correlation between spinal cord damage and neural cell apoptosis is not fully understood.

The present study was thus designed to investigate the localization of apoptotic cells, particularly neurons and oligodendrocytes, within the chronically compressed *twy/twy* mouse spinal cord as well as the potential role of tumor necrosis factor receptor 1(TNFR1), CD95 and $p75^{NTR}$ with neuronal and oligodendroglial apoptosis.

Materials and methods

Animal model

Experiments were conducted in 28 *twy/twy* mice (Central Institute for Experimental Animals, Kawasaki, Japan), aged 16 ($n = 9$) and 24 weeks ($n = 19$) and with a mean body weight of 29.5 ± 7.3 g (±SD). Mutant *twy/twy* mice were maintained by brother–sister mating of heterozygous Institute of Cancer Research (ICR) mice (+/*twy*). The disorder is inherited in an autosomal recessive manner and the homozygous hyperostotic mouse is identified by a characteristic tip–toe walking at 6–8 weeks of age, although no congenital neurological abnormalities are detected at that age. The spontaneous calcified deposits particularly in the atlantoaxial membrane grow progressively with age, causing profound motor paresis later in life. Figure 1 shows hematoxylin and eosin (H&E) stained sections of cervical spinal cord in 16-week-old (Fig. 1a) and 24-week-old (Fig. 1b, c) *twy/twy* mice. According to previous papers that analyzed the compressed transverse remnant area of the spinal cord (TRAS, %) using transaxial serial sections [3, 25], mice were divided into two groups based on the value of TRAS%: moderate compression

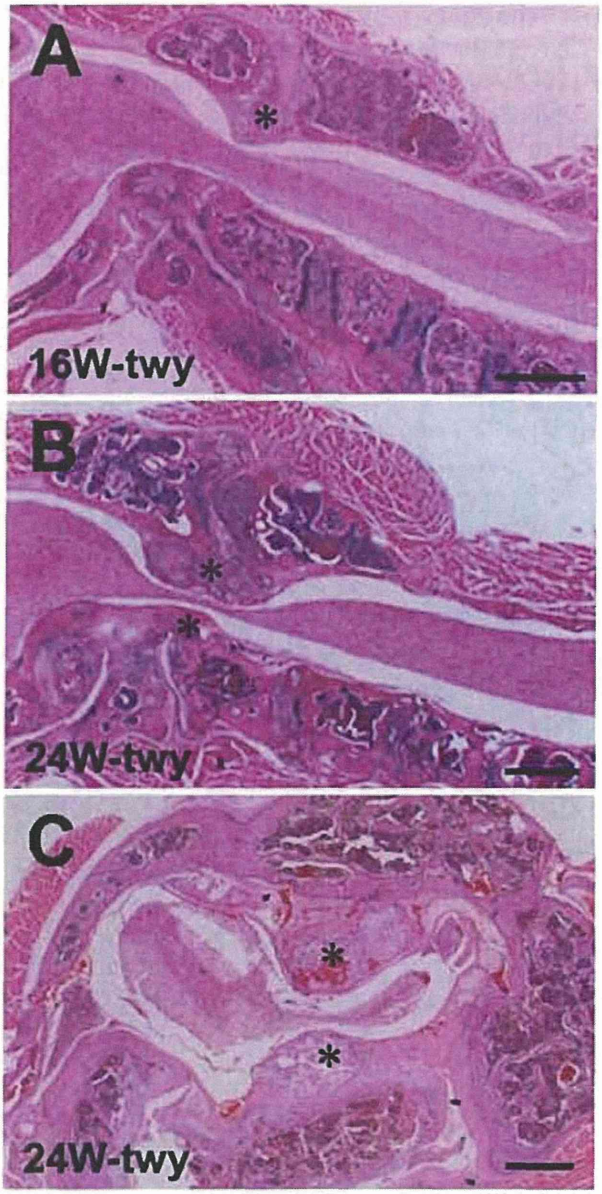

Fig. 1 Photographs showing representative hematoxylin and eosin (H&E)-stained sagittal (**a**, **b**) and transaxial (**c**) sections of the cervical spine and spinal cord in 16-week-old (**a**) and 24-week-old *twy/twy* mice (**b**, **c**). Calcified lesions originating from atlantoaxial membrane in *twy/twy* mice grow progressively with age, compressing the spinal cord between C2 and C3 segments laterally or posteriorly. *Asterisk* calcified lesions. *Scale bar* 500 μm (**a**, **b**), 200 μm (**c**)

group (TRAS% between 50 and 70%); and severe compression group (TRAS% ≤50%) in this study. ICR mice, age-matched with the *twy/twy* mice, were used as controls ($n = 12$) [3, 18]. The Ethics Review Committee for Animal Experimentation of Fukui University approved the experimental protocol.

Histology and measurement of demyelination in the spinal cord

Sections of the spinal cord were obtained for immunohistochemistry after intracardial perfusion were dehydrated through a graded ethanol series, and embedded in paraffin. They were then cut into 10-μm thick sections, deparaffinized in xylene and stained with H&E and luxol fast blue (LFB). For semi-quantitative analysis of demyelination, the LFB-positive areas in the ventro-lateral funiculus were analyzed by a color image analyzer (MacSCOPE; Mitani, Fukui, Japan). An area was considered LFB-positive area when the density significantly exceeded the threshold of the background; being calculated as percent cross-sectional area of the residual tissue [19].

Terminal deoxynucleotidyl transferase (TdT)-mediated dUTP-biotin nick end labeling (TUNEL) staining

Immediately after perfusion, the cervical cord was removed en bloc, postfixed, and then embedded in paraffin. Samples were cut in 4 μm-thick serial transverse sections. Deoxyribonucleic acid (DNA) fragmentation was detected by the TUNEL method using the ApopTag Peroxidase In Situ Apoptosis Detection kit (Chemicon International, Temecula, CA). The procedures used were performed as described in the kit manual. Color was developed using 3,3′-diaminobenzidine tetrachloride. Finally, the sections were counterstained with methyl green.

Immunoblot analysis

After cardiac arrest, the cervical spinal cord was immediately removed en bloc and stored in liquid nitrogen. The sample was solubilized in RIPA buffer, homogenized and then stored at −80°C. The protein concentration was analyzed by Bio-Rad DC protein assay kit (No. 500-0116, Bio-Rad Laboratories, Hercules, CA). Total protein (80 μg/lane) was subjected to sodium dodecylsulfate polyacrylamide gel (15%) electrophoresis (SDS-PAGE) and transferred onto polyvinylidene difluoride membrane in a semi-dry blot apparatus. The membranes were then washed twice in PBS, subsequently reacted with anti-TNFR1 (1:200, rabbit IgG; Santa Cruz Biotechnology, Santa Cruz, CA), anti-CD95 (1:1,000, rabbit IgG; Abcamn plc, Cambridge, UK) and anti-$p75^{NTR}$ (1:10; rabbit IgG; Abcamn plc) diluted overnight at 4°C sequentially by anti-rabbit IgG antibody and avidin-biotinylated peroxidase complex (1:200; Envision™ System-HRP Labeled Polymer, Dako Cytomation, Carpenteria, CA) for 3 h. After triple washing in 0.1 M PBS, the membrane was immersed and then subjected to radiography to visualize the peroxidase activity and thus level of antibody-binding. To quantify the relative level of expression of TNFR1, CD95 and $p75^{NTR}$ in ICR and *twy/twy* mice spinal cord, we analyzed the density of the bands on the photographic film with a densitometer using the NIH imaging software (ver. 1.59/ppc). Data were expressed in relative values as a semi-quantitative data, representing the ratio of each band density to β-tubulin (1:500, rabbit IgG; Abcamn plc).

Double immunofluorescence staining

To identify the type of apoptotic cells, double immunofluorescence staining was performed using frozen sections. Serial 25 μm-thick transverse frozen sections were treated with 0.1 M TRIS–HCl buffer (pH 7.6). For immunofluorescence staining, the sections were incubated at 4°C with anti-TNFR1 antibody (1:100, rabbit IgG; Santa Cruz Biotechnology), anti-CD95 antibody (1:50, rabbit IgG; Abcamn plc), and anti-$p75^{NTR}$ polyclonal antibody (1:100, rabbit IgG; Abcamn plc). The secondary antibodies were donkey anti-gout antibody Alexa Flour® 488/fluorescein-conjugated antibody (1: 250; Molecular Probes, Eugene, OR), and goat anti-rabbit Alexa Flour® 488/fluorescein-conjugated antibody (1:250; Molecular Probes) for 1 h at room temperature. For double immunofluorescence staining, the sections were further incubated with anti-neuronal nuclei monoclonal antibody (code No. MAB377, NeuN, 1:100, mouse IgG; Chemicon International), and anti-oligodendrocyte monoclonal antibody (code No. MAB1580, RIP, 1:100, mouse IgG; Chemicon International). The sections were then incubated with goat anti-mouse Alexa Flour® 568-conjugated antibody (1:250; Molecular Probes). The immunostained cells were visualized under confocal microscope equipped with a 15-mWatt crypton argon laser (model TCS SP2, Leica Instruments, Nussloch, Germany).

Statistical analysis

All values are expressed as mean ± SD. Differences between groups were examined for statistical significance using the paired t test. A P value < 0.05 denoted the presence of a significant difference. The above tests were conducted using The Statistical Package for Social Sciences software version 11.0 (SPSS, Chicago, IL).

Results

Histological evaluation of the mechanically compressed spinal cord

Luxol fast blue staining of the spinal cord (between C2 and C3 dorsal roots; the site of maximal compression) showed spongy necrosis spreading over the entire section of the spinal cord of the 16 and 24 weeks *twy/twy* mice but not the ICR mice ($n = 4$ in each group) (Fig. 2a). The differences were significant, especially in the marginal areas of the anterior and lateral columns. Further examination showed separation of the myelin sheath from the axon and axonal swelling and deformity; however, there was no severe degeneration, such as vascular degeneration or spongy degeneration, in the areas of compression. The percentage of the cross-sectional area of residual tissue was decreased with age, being significantly smaller than in the ICR mice (Fig. 2b).

TUNEL staining in the twy/twy mouse spinal cord

Figure 3a shows the topographic distribution of TUNEL-positive cells in the chronically compressed spinal cord of 16 and 24 weeks *twy/twy* mice ($n = 4$ in each group) examined by the TUNEL method. No TUNEL-positive cells were identified in both the grey and white matters of the control ICR mice spinal cord ($n = 2$). In contrast, TUNEL-positive cells were found in the gray and white matter in 16 weeks *twy/twy* mice. In comparison, fewer TUNEL-positive cells were found in 24 weeks *twy/twy* mice particularly in the anterior horn, though these cells remained abundant in the anterior columns. Figure 3b shows the results of comparative quantitative analysis of TUNEL-positive cells per sections in the anterior horn and anterior column at the maximal compressed spinal cord level in 16 and 24 weeks *twy/twy* mice ($n = 4$ in each group). In the spinal cord of 24 weeks *twy/twy* mice with severe compression, the number of TUNEL-positive cells was significantly higher in the anterior column compared with moderate compression mice.

Differences in expression of apoptotic signals between *twy/twy* and ICR mice

We evaluated the differences in the expression of various apoptotic signals between 24 weeks *twy/twy* mice ($n = 3$) and ICR ($n = 3$) mice by immunoblot analysis of the spinal cord. TNFR1, CD95, and $p75^{NTR}$ were overexpressed in *twy/twy* mice but not in ICR mice (Fig. 4a). Semi-quantitative analysis confirmed increased immunoreactivity to TNFR1, CD95, and $p75^{NTR}$ in *twy/twy* mice (Fig. 4b).

In sections double-stained for TNFR1, CD95, and $p75^{NTR}$ with NeuN and RIP, a number of double-stained cells were identified in the gray and white matters of 24-week-old *twy/twy* mice ($n = 6$). Although the number of neurons (gray matter) was lower in *twy/twy* mice than in ICR mice ($n = 3$), the expression of TNFR1, CD95, and $p75^{NTR}$ was mainly noted in the abundant oligodendrocytes (white matter) (Fig. 4c).

Discussion

Previous investigators have characterized the pathological features of chronically compressed spinal cords of patients

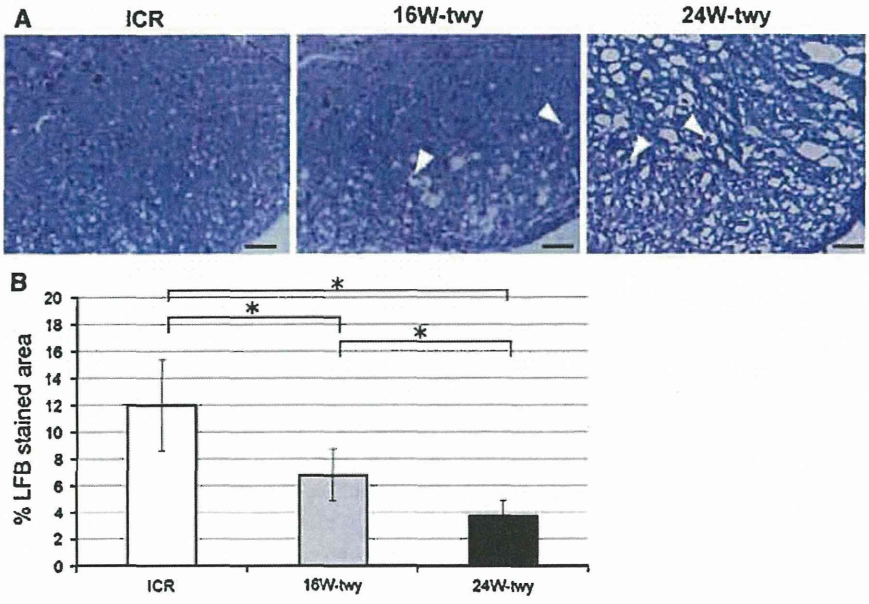

Fig. 2 Photographs showing representative LFB staining of the ventral microcystic cavity in 16 and 24 weeks *twy/twy* and ICR mouse. *Spotted white holes* caused by separation of myelin sheaths from the axons in the anterior and lateral columns in *twy/twy* mouse. Note also swelling and deformity (*arrow heads*) of axons particularly in the anterior columns in *twy/twy* mice (**a**). The percentage of the cross-sectional area of residual tissue was decrease with age in *twy/twy* mice and, being significantly smaller when compared with ICR mice (**b**). Data are mean ± SEM ($n = 4$). *$P < 0.05$

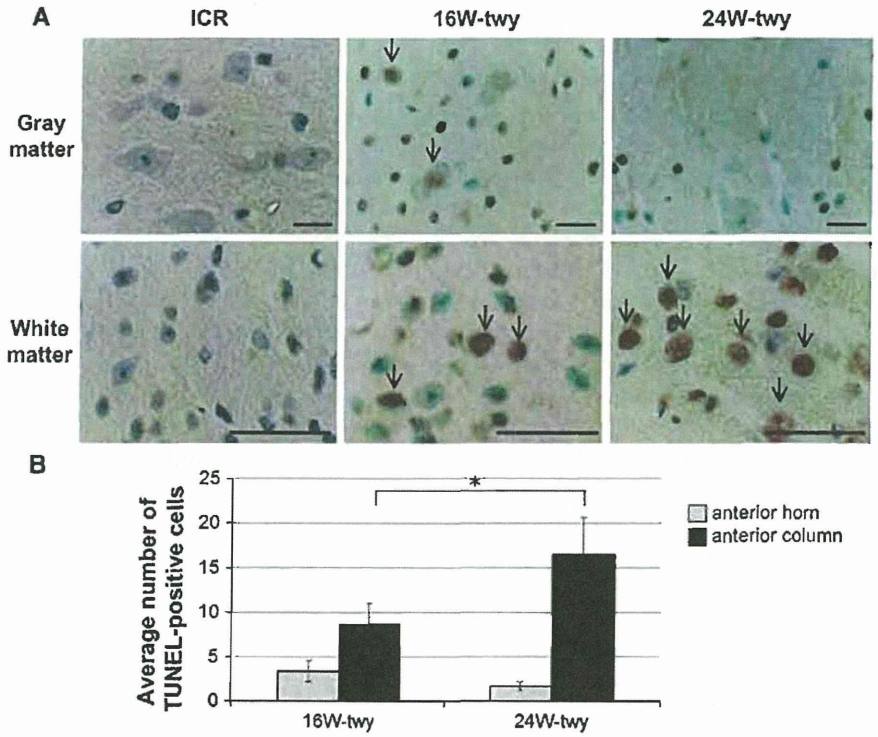

Fig. 3 Photomicrographs of terminal deoxynucleotidyl transferase (TdT)-mediated dUTP nick-end labeling (TUNEL) staining in representative control ICR (*left column*) mice and 16 weeks (*middle column*) and 24 weeks (*right column*) *twy/twy* spinal cord (a). Quantification of the number of TUNEL-positive cells at C1–C2 vertebral level of the 16 weeks *twy/twy* mice (moderate compression) and 24 weeks *twy/twy* mice (severe compression). The number of TUNEL-positive cells was higher in the anterior column in 24 weeks *twy/twy* mice compared with 16 weeks *twy/twy* mice. *Black arrows* representative TUNEL-positive cells. *Scale bar* 50 μm. Data are mean ± SEM ($n = 4$). *$P < 0.05$

with cervical myelopathy secondary to spondylosis or OPLL [9, 16, 30]. These studies indicated that spinal cord mechanical compression is characterized by the loss and exfoliation of anterior horn neurons with progressive spongy degeneration and demyelination in the white matter. In our previous publications, we observed a significant reduction in the number of remaining surviving neurons (Nissl stain-positive motoneurons) with reduction of TRAS of the *twy/twy* spinal cord to ≤70% of that of the control [3, 4]. Moreover, we also reported that the extent of demyelination and Wallerian degeneration in the white matter increased proportionately with the magnitude of spinal cord compression [25]. In the present study, examination of LFB-stained sections of the cervical spinal cord of the *twy/twy* mouse showed features of spongy necrosis over the entire section of the spinal cord, especially in the marginal areas of the anterior and lateral columns, compared with the ICR mice. We also found a clear decrease in TUNEL-positive cell count in both the anterior horn of the grey matter and the anterior column of the white matter in the maximally compressed spinal cord segment of the 24-week-old *twy/twy* mice with severe compression. Although TUNEL staining is not specific to apoptosis [11], because the staining also reflects necrosis, our finding suggests that neuronal loss in the anterior horn, after grey matter atrophy or together with spongy degeneration and demyelination of the white matter of *twy/twy* mouse spinal cord, is likely to be due to apoptotic death of neurons and glia.

After acute spinal cord injury, apoptosis of neurons and glial cells occurs rapidly at the level and vicinity of the traumatic insult, leading to a secondary pathologic cascade of neural injury. Several groups have concluded that neuronal cell apoptosis is the underlying process of spinal cord damage after traumatic injury [7, 10, 14]. Another study suggested the role of mitogen activated protein-kinase cascade in neuronal cell apoptosis of *twy/twy* mice, in addition to other yet unknown mechanism(s) [17]. In spinal cord injury, apoptotic oligodendrocytes are found along the spinal cord longitudinal axis both proximally and caudally far from the level of injury, but most significantly at and around the level of injury [1, 13, 19]. It has been reported that extensive damage of oligodendrocytes and neurons occurs initially at the site of trauma, followed by a second wave of injury, mainly evidenced by apoptotic oligodendrocytes in the white matter, in the following seven days; which spreads both proximally and caudally from the initial point of insult [14]. Axonal damage is followed by depletion of neurotrophic factors, which leads to apoptosis of oligodendrocytes present in the area distal to the spinal cord injury site [7]. A strong correlation has been found between the delayed axonal demyelination that follows spinal cord injury and apoptosis of oligodendrocytes [13]. In the present study, immunocytochemistry of double stained sections indicated that most of the apoptotic cells were oligodendrocytes. Though insignificant when compared to the acute spinal cord injury, the longitudinally

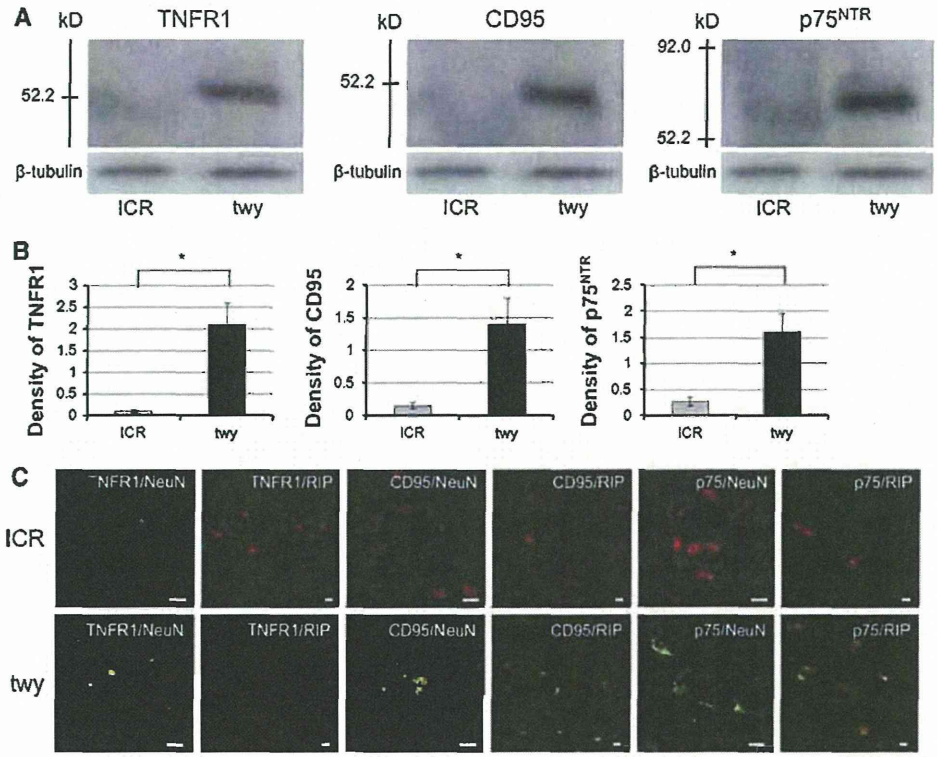

Fig. 4 Immunoblot analysis showing expression of TNFR1, CD95 and $p75^{NTR}$ (**a**) and photomicrographs of double-staining immunofluorescence (**c**). The intensity of the band in 24 weeks *twy/twy* mice (upper right on each panel, **a**) was significantly increased compared to that in ICR mice. Graphs indicate the band intensities relative to that of β-tubulin (**b**). The intensity of TNFR1, CD95 and $p75^{NTR}$ in the *twy/twy* mice was significantly higher than that of ICR mice. Data are mean ± SEM ($n = 3$). *$P < 0.05$. Photomicrographs show representative double-stained immunofluorescence in the gray and white matter of 24 weeks *twy/twy* and ICR mouse at the site between C2 and C3 dorsal roots (maximal compression site in *twy/twy* mouse) for TNFR1/NeuN, /RIP, CD95/NeuN, /RIP and $p75^{NTR}$/NeuN, /RIP. Note the double-positive cells in twy/twy mice. *Scale bar* 10 μm (**c**)

diffuse and extensive pattern of oligodendrocyte apoptosis in *twy/twy* mouse may be similar to the secondary damage process observed after acute trauma. Interestingly, the increment in the number of apoptotic cells in the *twy/twy* mouse was proportional to the magnitude of chronic external compression.

In the complex process of apoptosis, multiple signal transduction pathways are integrated [22, 28]. The effector phase of apoptosis involves the activation of caspases, a family of cysteine proteases that are activated through intrinsic and extrinsic pathways. Caspase-3 mediates the induction of apoptosis in spinal cord injury [21] with augmented expression of the death receptors as p75 receptors and especially Fas (CD 95) [5]. The p75 neurotrophin receptors are not only involved in the promotion of neuronal cell death [15] but also in neuronal survival [6]. On the other hand, it has been reported that the extrinsic pathway is activated via the ligand of cell surface death receptors belonging to the TNF/nerve growth factor receptor superfamily [2]. As an event of spinal cord injury, various cells (e.g., apoptotic neuronal and glial cells) over-express TNF-α [8], which seems to trigger apoptosis of oligodendrocytes [12]. A previous study suggested that apoptosis of oligodendrocytes may be induced by activated microglia through the secretion of various cytotoxic factors, including TNF-α, in response to axonal regeneration. It also has been reported that oligodendrocytes and possibly phagocytic microglia or macrophages comprised the population of apoptotic cells following spinal cord injury [20].

Double immunofluorescence staining in this study also indicated the expression of TNFR1, CD95 and $p75^{NTR}$ in local cells including neurons and oligodendrocytes, while apoptotic neurons and oligodendrocytes were identified by TUNEL staining in the segment with the most severe cord compression in the *twy/twy* mice. These results suggest the involvement of certain mechanisms in upregulation of inflammatory cytokines, including TNFR1, and that mechanical compression-induced expression of CD95 and $p75^{NTR}$ may closely contribute to apoptosis, particularly that of neurons and oligodendrocytes in the severe spinal cord compression observed in *twy/twy* mouse. These findings seem to follow a similar pattern to the human cervical

compressive myelopathy, which may validate the use of this animal model for the comparative study of such pathology in humans; making it suitable for the future assessment of the efficacy of the multiple therapeutics used in our patients as well as the study of the recovery mechanisms; in order to finally increase our knowledge of the human condition as our ultimate goal.

In conclusion, the present study demonstrated increased numbers of TUNEL-positive neurons in the gray matter and oligodendrocytes in the white matter of the spinal cord of the *twy/twy* mouse with progressive mechanical compression. Furthermore, the number of these cells increased with the magnitude of compression. Our immnohistochemical findings suggest that TNFR1, CD95 and $p75^{NTR}$ seem to play at least some role in the apoptotic process of neurons and oligodendrocytes, which probably contributes to axonal degeneration and demyelination in the *twy/twy* mouse spinal cord with severe compression.

Acknowledgments This work was supported in part by Grant-in-Aid to HB, HN and KU for General Scientific Research of the Ministry of Education, Science and Culture of Japan (grants numbers C17591558, B18390411, B21791389, and B22390287). This work was also supported in part by grants to HB from the Investigation Committee on Ossification of the Spinal ligaments, the Public Health Bureau of the Japanese Ministry of Labor, Health and Welfare (2005–2010).

Conflict of interest The authors declare no conflict of interest.

References

1. Abe Y, Yamamoto T, Sugiyama Y et al (1999) Apoptotic cells associated with Wallerian degeneration after experimental spinal cord injury: a possible mechanism of oligodendroglial death. J Neurotrauma 16:945–952
2. Ashkenazi A, Dixit VM (1998) Death receptor: signaling and modulation. Science 281:1305–1308
3. Baba H, Maezawa Y, Imura S et al (1996) Quantitative analysis of the spinal cord motoneuron under chronic compression: an experimental observation in the mouse. J Neurol 243:109–116
4. Baba H, Maezawa Y, Uchida K et al (1997) Three-dimensional topographic analysis of spinal accessory motoneurons under chronic mechanical compression: an experimental study in the mouse. J Neurol 244:222–229
5. Casha S, Yu WR, Fehlings MG (2001) Oligodendroglial apoptosis occurs along degenerating axons and is associated with FAS and p75 expression following spinal cord injury in the rat. Neuroscience 103:203–218
6. Chu GK, Yu W, Fehlings MG (2007) The p75 neurotrophin receptor is essential for neuronal cell survival and improvement of functional recovery after spinal cord injury. Neuroscience 148:668–682
7. Crowe MJ, Bresnahan JC, Shuman SL, Masters JN, Beattie MS (1997) Apoptosis and delayed degeneration after spinal cord injury in rats and monkeys. Nat Med 3:73–76
8. Inukai T, Uchida K, Nakajima H et al (2009) Tumor necrosis factor-alpha and its receptors contribute to apoptosis of oligodendrocytes in the spinal cord of spinal hyperostotic mouse (*twy/twy*) sustaining chronic mechanical compression. Spine 34:2848–2857
9. Kameyama T, Hashizume Y, Ando T et al (1995) Spinal cord morphology and pathology in ossification of the posterior longitudinal ligament. Brain 118:263–278
10. Katoh K, Ikata T, Katoh S et al (1996) Induction and its spread of apoptosis in rat spinal cord after mechanical trauma. Neurosci Lett 20:9–12
11. Koda M, Murakami M, Ino H et al (2002) Brain-derived neurotrophic factor suppresses delayed apoptosis of oligodendrocytes after spinal cord injury in rats. J Neurotrauma 19:777–785
12. Lee YB, Yune TY, Baik SY et al (2000) Role of tumor necrosis factor-alpha in neuronal and glial apoptosis after spinal cord injury. Exp Neurol 166:190–195
13. Li GL, Farooque M, Holtz A, Olsson Y (1999) Apoptosis of oligodendrocytes occurs for long distances away from the primary injury after compression trauma to rat spinal cord. Acta Neuropathol 98:473–480
14. Liu XZ, Xu XM, Hu R et al (1997) Neural and glial apoptosis after traumatic spinal cord injury. J Neurosci 17:5395–5406
15. Lowry KS, Murray SS, Coulson EJ et al (2001) Systemic administration of antisense p75(NTR) oligodeoxynucleotides rescues axotomised spinal cord neurons. J Neurosci Res 64:11–17
16. Mizuno J, Nakagawa H, Chang H-S et al (2005) Postmortem study of the spinal cord showing snake-eyes appearance due to damage by ossification of the posterior longitudinal ligament and kyphotic deformity. Spinal Cord 43:503–507
17. Nakahara S, Yone K, Sakou T et al (1999) Induction of apoptosis signal regulating kinase 1 (ASK1) after spinal cord injury in rats: possible involvement of ASK1-JNK and p38 pathways in neuronal apoptosis. J Neuropathol Exp Neurol 58:442–450
18. Okawa A, Nakamura I, Goto S et al (1998) Mutation in *Npps* in a mouse model of ossification of the posterior longitudinal ligament of the spine. Nat Genet 19:271–273
19. Shi X, Kang Y, Hu Q et al (2010) A long-term observation of olfactory ensheathing cells transplantation to repair white matter and functional recovery in a focal ischemia model in rat. Brain Res 1317:257–267
20. Shuman SL, Bresnahan JC, Beattie MS (1997) Apoptosis of microglia and oligodendrocytes after spinal cord contusion in rats. J Neurosci Res 50:798–808
21. Springer JE, Azbill RD, Knapp PE (1999) Activation of the caspase-3 apoptotic cascade in traumatic spinal cord injury. Nat Med 5:943–946
22. Takenouchi T, Setoguchi T, Yone K, Komiya S (2008) Expression of apoptosis signal-regulating kinase 1 in mouse spinal cord under chronic mechanical compression: possible involvement of the stress-activated mitogen-activated protein kinase pathways in spinal cord cell apoptosis. Spine 33:1943–1950
23. Uchida K, Baba H, Maezawa Y et al (1998) Histological investigation of spinal cord lesions in the spinal hyperostotic mouse (*twy/twy*): morphological changes in anterior horn cells and immunoreactivity to neurotrophic factors. J Neurol 245:781–793
24. Uchida K, Baba H, Maezawa Y et al (2003) Increased expression of neurotrophins and their receptors in the mechanically compressed spinal cord of the spinal hyperostotic mouse (*twy/twy*). Acta Neuropathol 106:29–36

25. Uchida K, Baba H, Maezawa Y, Kubota C (2002) Progressive changes in neurofilament proteins and growth-associated protein-43 immunoreactivities at the site of cervical spinal cord compression in spinal hyperostotic mice. Spine 27:480–486
26. Uchida K, Nakajima H, Inukai T et al (2008) Adenovirus-mediated retrograde transfer of neurotrophin-3 gene enhances survival of anterior horn neurons of *twy/twy* mice with chronic mechanical compression of the spinal cord. J Neurosci Res 86:1789–1800
27. Xu K, Uchida K, Nakajima H, Kobayashi S, Baba H (2006) Targeted retrograde transfection of adenovirus vector carrying brain-derived neurotrophic factor gene prevents loss of mouse (*twy/twy*) anterior horn neurons in vivo sustaining mechanical compression. Spine 31:1867–1874
28. Yamaura I, Yone K, Nakahara S et al (2002) Mechanism of destructive pathologic changes in the spinal cord under chronic mechanical compression. Spine 27:21–26
29. Yu WR, Baptiste DC, Liu T et al (2009) Molecular mechanisms of spinal cord dysfunction and cell death in the spinal hyperostotic mouse: implications for the pathophysiology of human cervical spondylotic myelopathy. Neurobiol Dis 33:149–163
30. Yu YL, Leong JC, Fang D et al (1988) Cervical myelopathy due to ossification of the posterior longitudinal ligament. A clinical, radiological and evoked potentials study in six Chinese patients. Brain 111:769–783

Spine

SPINE Volume 36, Number 17, pp 1350–1358

BASIC SCIENCE

Tumor Necrosis Factor-α Antagonist Reduces Apoptosis of Neurons and Oligodendroglia in Rat Spinal Cord Injury

Ke-Bing Chen, MD,*† Kenzo Uchida, MD, PhD,* Hideaki Nakajima, MD, PhD,* Takafumi Yayama, MD, PhD,* Takayuki Hirai, MD,* Shuji Watanabe, MD,* Alexander Rodriguez Guerrero, MD,*‡ Shigeru Kobayashi, MD, PhD,* Wei-Ying Ma, MD,*†§ Shao-Yu Liu, MD, PhD,† and Hisatoshi Baba, MD, PhD*

Study Design. To examine the effects of a tumor necrosis factor (TNF)-α antagonist (etanercept) on rat spinal cord injury and identify a possible mechanism for its action.

Objective. To elucidate the contribution of etanercept to the pathologic cascade in spinal cord injury and its possible suppression of neuronal and oligodendroglial apoptosis.

Summary of Background Data. Etanercept has been recently used successfully for treatment of inflammatory disorders. However, only a few studies have examined its role in suppressing neuronal and oligodendroglial apoptosis in spinal cord injury.

Methods. Etanercept or saline (control) was administered by intraperitoneal injection 1 hour after thoracic spinal cord injury in rats. The expressions and localizations of TNF-α, TNF receptor 1 (TNFR1), and TNF receptor 2 (TNFR2) were examined by immunoblot and immunohistochemical analyses. Spinal cord tissue damage between saline- and etanercept-treated groups was also compared after hematoxylin-eosin and luxol fast blue (LFB) staining. The Basso-Beattie-Bresnahan (BBB) scale was used to evaluate rat locomotor function after etanercept administration. Terminal deoxynucleotidyl transferase (TdT)-mediated dUTP-biotin nick end labeling (TUNEL)-positive cells were counted and the immunoreactivity to active caspase-3 and caspase-8 was examined after etanercept administration.

Results. Immunoblot and double immunofluorescence staining revealed suppression of TNF-α, TNFR1, and TNFR2 expression after administration of etanercept in the acute phase of spinal cord injury. LFB staining demonstrated potential myelination in the etanercept-treated group from 2 week after spinal cord injury, together with an increased BBB locomotor score. Double immunofluorescence staining showed a significant decrease in TUNEL-positive neurons and oligodendroglia from 12 hour to 1 week in the gray and white matters after etanercept administration. Immunoblot analysis demonstrated overexpression of activated caspase-3 and caspase-8 after spinal cord injury, which was markedly inhibited by etanercept.

Conclusion. Our results indicated that etanercept reduces the associated tissue damage of spinal cord injury, improves hindlimb locomotor function, and facilitates myelin regeneration. This positive effect of etanercept on spinal cord injury is probably attributable to the suppression of TNF-α, TNFR1, TNFR2, and activated caspase-3 and caspase-8 overexpressions, and the inhibition of neuronal and oligodendroglial apoptosis.

Key words: apoptosis, neurons, oligodendroglia, spinal cord injury, tumor necrosis factor (TNF)-alpha, etanercept. **Spine 2011; 36:1350–1358**

Traumatic spinal cord injury initiates a complex series of cellular and molecular events that induce massive cell death of neurons and glial cells, extensive demyelination, and axonal destruction, leading to permanent neurologic deficits. Several studies demonstrated the rapid appearance of apoptotic neurons and glial cells in injured cord segments and adjacent areas after spinal cord injury.[1–4] Programmed cell death of oligodendroglia was also observed along the longitudinal axis of the spinal cord, possibly contributing to the delayed and prolonged demyelination process that leads to deterioration of spinal cord sensorimotor function.[3,5] Prevention of apoptosis after spinal cord injury could therefore potentially lead to spinal cord tissue repair and improved motor function. Indeed, a number of experiments have attempted to suppress apoptotic cell death after spinal cord injury.[6–8]

From the *Department of Orthopaedics and Rehabilitation Medicine, Faculty of Medical Sciences, University of Fukui, Japan; †Department of Spinal Surgery, The First Affiliated Hospital, Sun Yat-Sen University, People's Republic of China; ‡Servicio de Neurocirugia, Hospital Nacional Rosales, Universidad de El Salvador, San Salvador, El Salvador; and §Department of Anaesthesiology, The Second Affiliated Hospital, Sun Yat-Sen University, Guangzhou 510120, People's Republic of China.

Acknowledgment date: May 17, 2010. First revision date: June 22, 2010. Acceptance date: June 29, 2010.

The manuscript submitted does not contain information about medical device(s)/drug(s).

No benefits in any form have been or will be received from a commercial party related directly or indirectly to the subject of this manuscript.

Supported in part by grants-in-aid to HB, HN, and KU for General Scientific Research of the Ministry of Education, Science and Culture of Japan (grants number B18390411, B19791023, C21591895, C21791389, and B22390287).

This work was also supported by grants from the Investigation Committee on Ossification of the Spinal Ligaments (2005–2010) and Research Program for Spinal Cord Intractable Pain (2009–2010).

Address correspondence and reprint requests to Kenzo Uchida, MD, PhD, Department of Orthopaedics and Rehabilitation Medicine, Faculty of Medical Sciences, University of Fukui, Matsuoka Shimoaizuki 23-3, Eiheiji, Fukui 910-1193, Japan; E-mail: kuchida@u-fukui.ac.jp

DOI: 10.1097/BRS.0b013e3181f014ec